Lifetime measurements and magnetic rotation in ^{107}Ag

S. H. Yao,[1] H. L. Ma,[1] L. H. Zhu,[2,*] X. G. Wu,[1,†] C. Y. He,[1] Y. Zheng,[1] B. Zhang,[1,3] G. S. Li,[1] C. B. Li,[1,4] S. P. Hu,[1,3] X. P. Cao,[1,5] B. B. Yu,[1] C. Xu,[6] and Y. Y. Cheng[6]

[1]*China Institute of Atomic Energy, Beijing 102413, China*

[2]*School of Physics and Nuclear Energy Engineering, Beihang University, Beijing 100191, China*

[3]*College of Physics and Technology, Shenzhen University, Shenzhen 518060, China*

[4]*College of Physics, Jilin University, Changchun 130012, China*

[5]*Department of Physics, Northeast Normal University, Changchun 130024, China*

[6]*School of Physics and State Key Laboratory of Nuclear Physics and Technology, Peking University, Beijing 100871, China*

(Received 29 September 2013; revised manuscript received 2 January 2014; published 29 January 2014)

The excited states in ^{107}Ag were populated through the heavy-ion fusion evaporation reaction ^{100}Mo (^{11}B, $4n$) ^{107}Ag at a beam energy of 46 MeV. Lifetimes of high-spin states in ^{107}Ag have been measured through the Doppler shift attenuation method. The deduced $B(M1)$ values, gradually decreasing with increasing spin, clearly demonstrate that both the yrast positive-parity band and the yrast negative-parity band in ^{107}Ag are magnetic rotation bands. Furthermore, experimental deduced $B(M1)$ values for the yrast positive-parity band are compared with the predictions of the particle rotor model. The approximate agreement between theoretical calculations and experimental results further confirms the mechanism of magnetic rotation for the yrast positive-parity band. In addition, a systematic investigation shows the evolution of the magnetic rotation mechanism in the $A \approx 110$ mass region.

DOI: 10.1103/PhysRevC.89.014327 PACS number(s): 21.10.Re, 23.20.Lv, 21.10.Tg, 21.60.Ev

I. INTRODUCTION

Since the first observation of magnetic rotational bands in Pb isotopes in the early 1990s, a large number of magnetic bands have been observed in spherical or near-spherical nuclei in $A \approx 80,110,140,190$, and 60 mass regions [1,2]. The magnetic rotational bands should involve coupling of high-j valence proton particles (holes) and high-j valence neutron holes (particles). The angular-momentum vectors of the particles and holes are nearly perpendicular to each other at the bandhead. The band angular momentum is generated by gradual alignment of the particles and holes angular-momentum vectors towards the total angular-momentum vector. The magnetic moment vector rotates around the total angular-momentum vector and results in a perpendicular component, $\mu_\perp$, which is large at the bandhead and decreases as total angular momentum gradually increases. Therefore, the $B(M1)$ values also decrease with increasing angular momentum, which is a vital experimental proof of a magnetic rotational band. Magnetic rotational or antimagnetic bands have been identified in Rh, Ag, Cd, In, Sn, and Sb isotopes in the $A \approx 110$ mass region where the nuclei involve coupling of one or more proton holes in the high-Ω $g_{9/2}$ orbitals with neutrons in the low-Ω $g_{7/2}$, $d_{5/2}$, and $h_{11/2}$ orbitals. Magnetic rotational bands are also expected in ^{107}Ag, in addition to $^{103-106}$Ag [3–7] and ^{109}Ag [8] in Ag isotopes. The level scheme of ^{107}Ag has been reported previously [9–11]. In this work, lifetime measurements have been performed for high-spin states of the yrast positive-parity band and the yrast negative-parity band in ^{107}Ag. The corresponding $M1$ and $E2$ transitional strengths have been deduced for the discussion of magnetic rotation with the help of theoretical calculations and systematic arguments.

II. EXPERIMENTS AND RESULTS

The experiment was carried out at the HI-13 tandem accelerator in the China Institute of Atomic Energy. The high-spin states of ^{107}Ag were populated via the heavy-ion fusion evaporation reaction ^{100}Mo (^{11}B, $4n$) ^{107}Ag at a beam energy of 46 MeV. The target consisted of 0.97-mg/cm^2-thick, isotopically enriched, ^{100}Mo foil backed by a 8.8-mg/cm^2-thick layer of natural Yb in order to slow down and stop the recoiling nuclei. An array consisting of 12 Compton-suppressed HPGe detectors and two planar HPGe detectors were employed to detect the deexcited γ rays from the reaction residues. The HPGe detectors in the array were placed, with respect to the beam direction, as follows: five at 90°, two at 42°, two at 140°, three at about 150°, one at 127°, and one at 34°. Each HPGe detector has an energy resolution of about 2 keV for the 1332.5-keV γ ray. Energy and efficiency calibration of the HPGe detectors ware performed using ^{60}Co, ^{133}Ba, and ^{152}Eu standard radioactive sources. About 6.5×10^7 coincidence events were accumulated in the event-by-event mode.

After careful gain matching of all the spectra of detectors, the recorded γ-γ coincidence data were sorted into a fully symmetrical E_γ-E_γ matrix as well as into several asymmetric matrices. Symmetrical E_γ-E_γ matrix was used to determine branching ratios and side-feeding intensities for states being studied. The asymmetric matrices, with one detector at 150° or 42° on one axis, respectively, versus four detectors at 90° on the other axis were sorted to generate γ-ray spectra used in the process of lifetime analysis. These matrices were analyzed using the RADWARE package [12] based on a Linux PC system.

*Corresponding author: zhulh@buaa.edu.cn

†Corresponding author: wxg@ciae.ac.cn

The lifetimes of high-spin states in ^{107}Ag were extracted from the analysis of Doppler-broadened line shapes using the DSAMFT analysis program developed by Gascon [13]. Line shapes were observed at 150° or 42° while gates were applied at 90°. Gating transitions were set at the full peak shape of the cascades following the γ transitions for which the Doppler-broadened line shape was observed. Meanwhile, the gating transitions were judiciously chosen to obtain spectra with the least contaminant transitions. Generally, the gated spectra were summed to obtain better statistic precision. The velocity profile of the recoiling nuclei traversing the target and the backing material was simulated with a Monte Carlo procedure. Stopping powers of beam in target, recoils in target and recoils in backing were calculated according to the model given by Ziegler *et al*. [14]. The intensity of side-feeding and the branch ratios of transition were deduced from the above symmetrical matrix. Lifetimes were then extracted from a χ^2 minimization process for fitting line shapes of the gated γ rays depopulating the levels of interest. The final values for the levels lifetimes were obtained by taking the averages from the fits of line shapes at 150° and 42°.

The partial level scheme of ^{107}Ag established from the present work is shown in Fig. 1. It confirms the major part of the ^{107}Ag level scheme known from Refs. [9–11]. The labeling of the bands is kept the same as in Ref. [9] to simplify the discussion, where band 1 represents the yrast positive-parity band and band 3 the negative-parity band. The lifetimes of levels from $25/2^+$ to $35/2^+$ in band 1 and from $23/2^-$ to $29/2^-$ in band 3 were extracted. The representative examples of line-shape fits observed at the forward (42°) and the backward (150°) angles with respect to the beam direction are shown in Fig. 2. The experimental reduced transition probabilities, $B(M1)$ and $B(E2)$ values, were obtained from lifetimes by the following expressions [15]:

$$B(M1) = \frac{0.056\,97 B_{\gamma_1}}{E_{\gamma_1}^3 \tau [1 + \alpha_t(M1)]} [\mu_N^2], \quad (1)$$

$$B(E2) = \frac{0.081\,56 B_{\gamma_2}}{E_{\gamma_2}^5 \tau [1 + \alpha_t(E2)]} [(eb)^2], \quad (2)$$

where E_{γ_1} and E_{γ_2} are the γ-ray energy in MeV of the $M1$ and $E2$ transitions, respectively, τ is the level lifetime in ps, and $\alpha_t(M1)$ and $\alpha_t(E2)$ are the total theoretical internal conversion coefficients [16]. The branching ratios B_{γ_1} and B_{γ_2} are obtained from the measured γ-ray intensities of the $M1$ and crossover $E2$ transitions. The lifetimes, $B(M1)$, and $B(E2)$ values for both band 1 and band 3 in ^{107}Ag are tabulated in Table I. Systematic errors in the stopping power values are included in the quoted errors and may be as large as 15%.

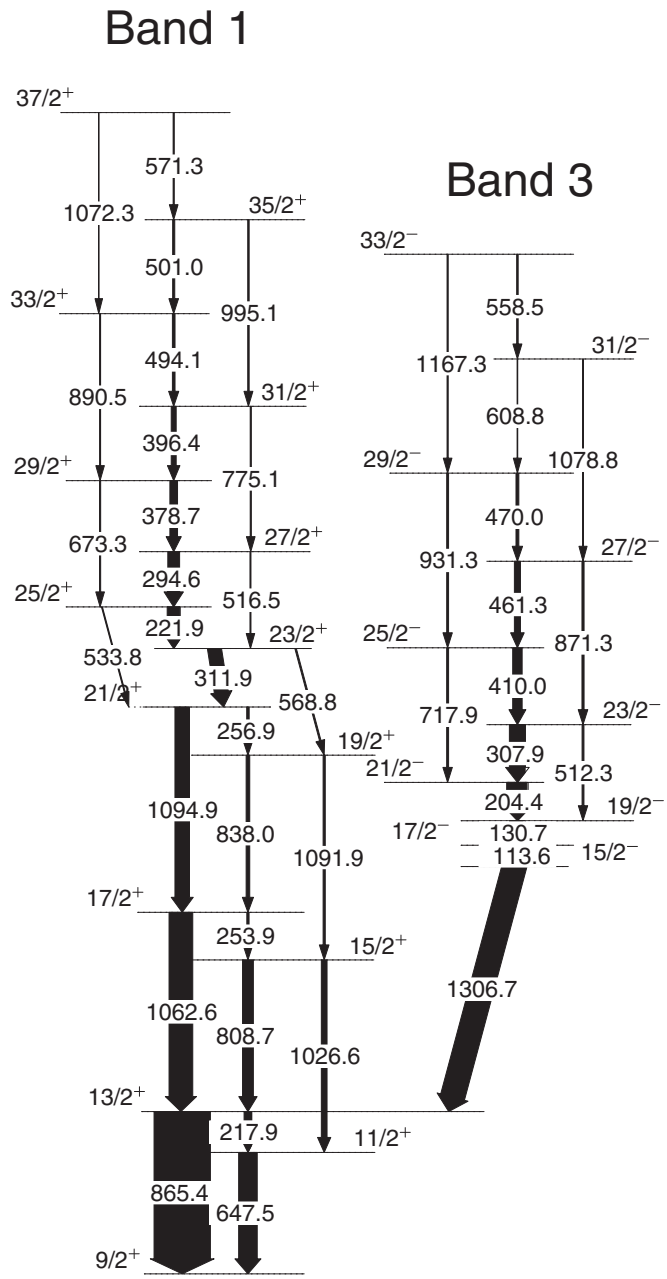

FIG. 1. Partial level scheme of ^{107}Ag obtained from the present work. The energies are given in keV; the width of the transitions are proportional to their relative intensities.

III. DISCUSSION

The theoretical discussion on the magnetic bands are usually based on the tilted-axis cranking (TAC) model [17,18] or the particle rotor model (PRM) [19–21]. There are also attempts on the tilted-axis cranking of the self-consistent mean-field theories [22–24]. In Ref. [20], a many-particles-plus-rotor model without pairing was developed and used in the study on the shear mechanism in ^{198,199}Pb. In this paper, we use this many-particles-plus-rotor model to investigate the positive-parity band in ^{107}Ag. The deformation parameters of the rotor will be taken from the theoretical calculations by the cranked Nilsson Strutinsky (CNS) approach. The CNS approach without pairing has been highly successful in describing the high-spin rotational structures in the whole nuclear chart [25,26]. Following the first backbending in the yrast positive-parity band of ^{107}Ag, the neutron pairing correlation would be greatly hindered due to the alignment of two quasineutrons. And the proton pairing correlation is also

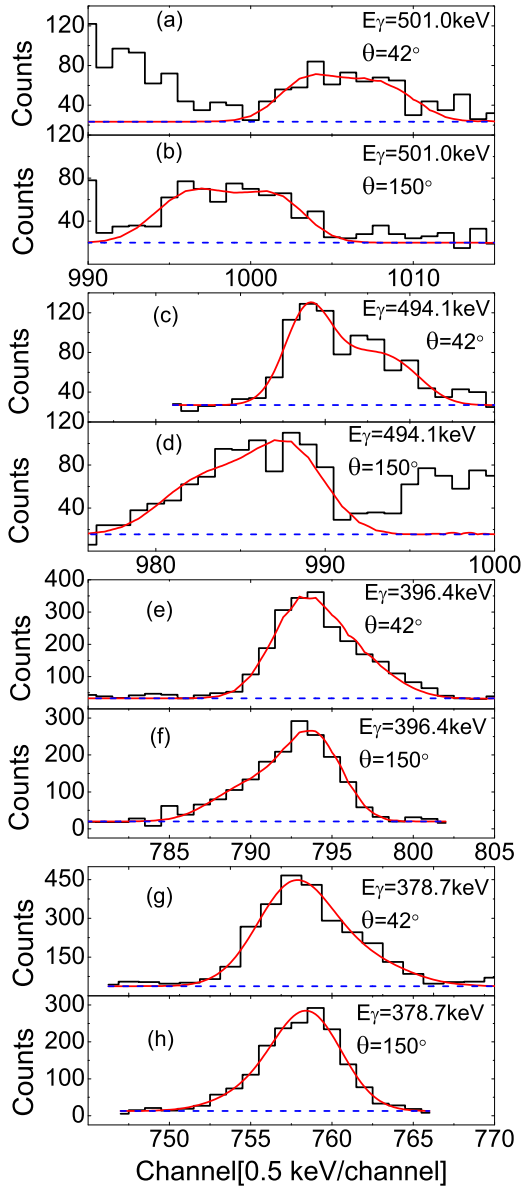

FIG. 2. (Color online) Examples of the line-shape fits for 501.0, 494.1, 396.4, and 378.7 keV transitions at 150° and 42° with respect to the beam direction.

weak because of the existence of the $Z = 46(48)$ gap and the blocking effect of the single proton. Therefore, the unpaired CNS approach could provide a reliable information on the rotational structure of ^{107}Ag.

The CNS calculations were first carried out in a quadrupole and hexadecapole deformation mesh $(\varepsilon_2,\gamma,\varepsilon_4)$ with the standard Nilsson parameters [27]. In our calculations, the $\pi(1g_{9/2})^7 \otimes \nu[(2d_{5/2}1g_{7/2})^8(1h_{11/2})^2]$ configuration is found to be energy favored. The theoretical results are compared with the experimental data in Fig. 3. It is seen that the experimental data after the backbending are fairly well reproduced. The quadrupole deformation calculated in the intermediate spin region $23/2\hbar \leqslant I \leqslant 41/2\hbar$ is $0.17 \lesssim \varepsilon_2 \lesssim 0.19$ with slight triaxial deformation $0° < \gamma < 10°$. That explains the vanishing signature splitting after the backbending. However, the

TABLE I. Measured lifetimes and the corresponding $B(M1)$ and $B(E2)$ values for both band 1 and band 3 in ^{107}Ag.

Band	I^π ($\hbar$)	E_γ (keV)	τ (ps)	$B(E2)$ (e^2b^2)	$B(M1)$ (μ_N^2)
Band 1	$25/2^+$	221.9	0.88(38)	0.15(7)	5.2(23)
	$27/2^+$	294.6	0.75(15)	0.23(5)	2.7(6)
	$29/2^+$	378.7	0.50(8)	0.15(3)	1.8(3)
	$31/2^+$	396.4	0.39(5)	0.14(3)	1.9(3)
	$33/2^+$	494.1	0.17(3)	0.23(6)	1.9(4)
	$35/2^+$	501.0	<0.21[a]	>0.16	>1.25
Band 3	$23/2^-$	307.9	1.36(39)	0.18(6)	1.25(36)
	$25/2^-$	410.0	0.83(17)	0.09(2)	0.82(18)
	$27/2^-$	461.3	0.50(9)	0.08(2)	0.85(17)
	$29/2^-$	470.0	<0.83[a]	>0.06	>0.39

[a]Effective lifetime not corrected for feeding.

signature splittings before the backbending are not reproduced. In a paired study with the cranked-Nilsson-Strutinsky-Bogoliubov approach, the calculated deformation before the backbending is $\varepsilon_2 \sim 0.15$ and $\gamma \sim -10°$, which would result in a significant energy splitting between the two signature partner bands. After the alignment of two $h_{11/2}$ quasineutrons, the additional driving force will drive the ^{107}Ag nucleus to a larger quadrupole deformed shape with slight positive γ,

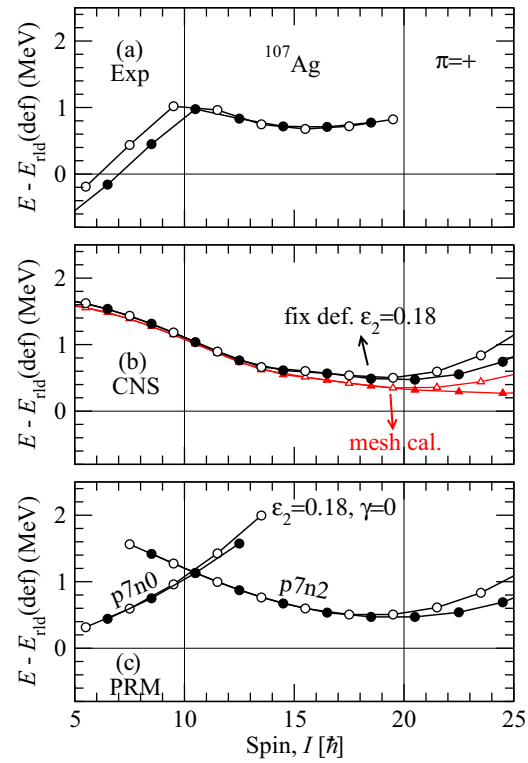

FIG. 3. (Color online) Experimental and theoretical rotational energies of the positive-parity bands respect to the rotational rigid body reference. In the CNS calculations, the deformation parameters are taken as $(\varepsilon_2,\gamma,\varepsilon_4) = (0.18,0.0,0.0)$ with the configuration $\pi(1g_{9/2})^7 \otimes \nu[(2d_{5/2}1g_{7/2})^8(1h_{11/2})^2]$. The PRM results have been normalized to roughly give the CNS results.

and the calculated deformation is consistent with the previous unpaired CNS calculations. In spite of some difference in the deformation parameters before and after the backbending, in the following we will neglect that difference for simplicity and discuss the rotational structure of the yrast positive-parity bands at the sole deformation, i.e., $(\varepsilon,\gamma) = (0.18,0.0^\circ)$. It is shown in Fig. 3 that the energies at the fixed deformation are very close to those in the mesh calculation for $I \leqslant 39/2\hbar$, thus it is reasonable to set this deformation to the core rotor in the following PRM calculations.

In the PRM calculation, $^{100}_{40}$Zr and $^{98}_{40}$Zr will be taken as the core for the bands before and after the backbending, respectively. The seven valence protons will occupy the $g_{9/2}$ orbitals and, in the case of the ^{98}Zr core, an additional two neutrons will sit in the $h_{11/2}$ orbitals. These two setups are denoted as $p7n0$ and $p7n2$, respectively. In order to obtain the moments of inertia (MOI) of the core, the rotational energies of ^{98}Zr are fitted with the following formula:

$$E_{\rm rotor} = \frac{1}{2\mathcal{J}} I(I+1) + E_0^{\rm rot}, \tag{3}$$

where $E_{\rm rotor}$ are calculated by the principle axis cranking model. However, the Strutinsky smearing procedure is not carried out in this stage to avoid the double counting. The linear fitting of $E_{\rm rotor}$ using Eq. (3) gives $\mathcal{J} = 12.62\hbar^2/\text{MeV}$. The moments of inertia along three axes are assumed to be connected by a relationship of hydrodynamical type. In the present choice of the symmetric rotor, $\mathcal{J}_1 = \mathcal{J}_2 = \mathcal{J}$ and $\mathcal{J}_3 = 0$. The MOI of $^{100}_{40}$Zr is set as the same as that of $^{98}_{40}$Zr since two isotopes differ by only one pair of neutrons and their MOIs are expected to be very close to each other.

In the cranking shell-model calculations, the energy is usually Strutinsky renormalized to the average behavior of a liquid-drop model. In order to compare the energies calculated by the PRM and the CNS calculations, similar smearing procedure should be performed [20]. The rigid body and Strutinsky smoothed moment of inertias are calculated by the CNS code, which gives $\mathcal{J}_{\rm rig} = 37.59\hbar^2/\text{MeV}$ and $\mathcal{J}_{\rm str} = 46.73\hbar^2/\text{MeV}$ for ^{107}Ag at $(\varepsilon_2,\gamma,\varepsilon_4) = (0.18,0.0,0.0)$. Figure 3(c) gives the PRM rotational energies in ^{107}Ag. The results have been renormalized to roughly agree with the CNS results while the $p7n0$ results are renormalized to give the same energy at $21/2\hbar$ as the $p7n2$ configuration. The PRM results of the $p7n2$ configuration agree well with the CNS calculations at the fixed deformation.

In the PRM calculation of magnetic transitions, the effective gyromagnetic factors are taken to be $g_R = Z/A = 0.44$ for the rotor and $g_s^{\rm eff} = 0.7 g_s$ for the valence nucleons. In Fig. 4(a), the theoretical $B(M1)$ values are compared with the experimental data. By putting two $1h_{11/2}$ neutrons in the valence space, the $M1$ transitions are largely enhanced for the $p7n2$ configuration compared with the $p7n0$ configuration. From experimental and theoretical data, it can be seen that the $B(M1)$ values lie in the range of 1–5μ_N^2 and they decrease with increasing spin. As is known, a decreasing trend of the $B(M1)$ values with increasing spin provides a crucial test for the magnetic rotation. Both experimental and theoretical $B(E2)$ values, shown in Fig. 4(b), lie in the range of 0.1–0.2 e^2b^2, which is the character of magnetic rotation. Furthermore, the moment

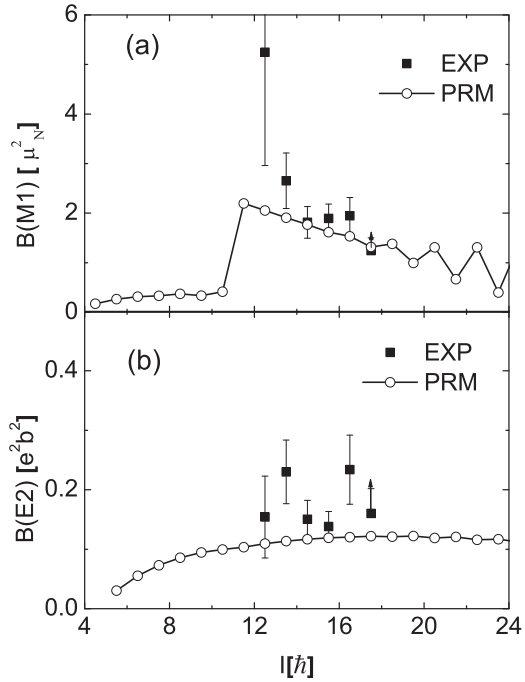

FIG. 4. Experimental and theoretical $B(M1)$ and $B(E2)$ values. The experimental data are taken from the present work. The PRM results for $I \leqslant 21/2\hbar$ and $I \geqslant 23/2\hbar$ are calculated with the configuration $p7n0$ and $p7n2$, respectively.

of inertia, $\mathcal{J}^{(2)} \sim 20\ \hbar^2\ \text{MeV}^{-1}$, and the ratios of the moment of inertia to the reduced $E2$ transition probability, $\mathcal{J}^{(2)}/B(E2) \sim 100\ \text{MeV}^{-1}\ e\text{b}^{-1}$, also meet the expectation of magnetic rotation. However, the staggering of the spins I as a function of rotational frequency ω, as is shown in Fig. 5(d), indicates that band 1 has a significant contribution from collective rotation. Since the staggering is usually associated with signature splitting, which is a well-established phenomenon

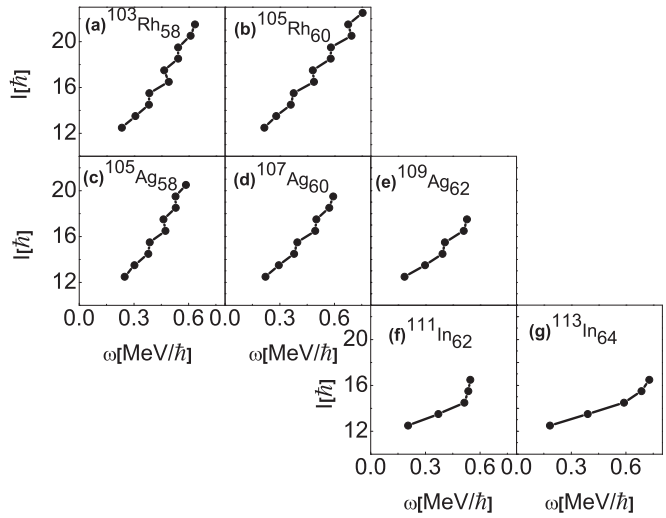

FIG. 5. Angular momentum as a function of rotational frequency ω for band 1 in ^{107}Ag as well as bands with the configuration $\pi g_{9/2} \otimes h_{11/2}{}^2$ in ^{103,105}Rh, ^{105,109}Ag, and ^{111,113}In.

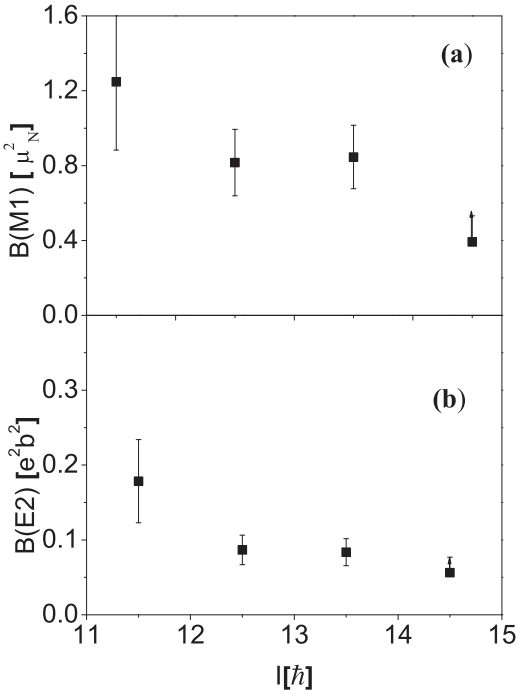

FIG. 6. Experimental $B(M1)$ and $B(E2)$ values as the function of angular momentum for band 3.

for collective rotations in well-deformed nuclei and cannot be associated with magnetic rotation. The observed spins I for the bands with the configuration $\pi g_{9/2}\otimes h_{11/2}{}^2$ in Rh [28,29], Ag [6,8], and In [30–33] isotopes are also plotted in Fig. 5. The staggering is evident in Rh isotopes and becomes smaller in Ag isotopes and finally vanishes in In isotopes. One can see the evolution that contribution from magnetic rotation increases and contribution from collective rotation decreases with the growing number of proton towards proton magic number 50 or with the growing number of $h_{11/2}$ neutrons.

For the negative-parity bands, the $\pi(1g_{9/2})^7 \otimes \nu[(2d_{5/2}1g_{7/2})^9(1h_{11/2})^1]$ configuration is energy favored in the CNS calculations. The quadrupole deformation is somewhat less than the positive-parity $\pi(1g_{9/2})^7 \otimes \nu[(2d_{5/2}1g_{7/2})^8(1h_{11/2})^2]$ configuration because the deformation driving force will be weaker with only one neutron occupying the low-Ω high-j $1h_{11/2}$ orbitals. The calculated deformation is nearly a prolate shape and $\varepsilon_2 \sim 0.15$ for $I \sim 31/2\hbar$. Hence, it is expected that the $B(E2)$ values of band 3 are less than that of band 1 at the same spin, which is consistent with our observations. However, because of the complexity brought by the three unpaired nucleons, the calculation is beyond the current PRM capacities. The experimental $B(M1)$ values are very large while the experimental $B(E2)$ values are small, and $B(M1)$ values also exhibit a decreasing trend with increasing spin, as shown in Fig. 6. Moreover, the moment of inertia, $\mathcal{J}^{(2)}$, is generally of the order of $20\hbar^2$ MeV^{-1} while the ratios of the moment of inertia to the reduced $E2$ transition probability, $\mathcal{J}^{(2)}/B(E2)$, is of the order of 200 MeV^{-1} eb^{-1}. Therefore, band 3 is also interpreted as a magnetic rotation band. The evolution of magnetic rotation with the growing number of neutrons can also be observed for bands with the configuration $\pi g_{9/2}\otimes[h_{11/2}(g_{9/2}/d_{5/2})^1]$ in ^{103,105,107}Ag, which was reproduced by the TAC model in Ref. [34].

IV. SUMMARY

To summarize, lifetimes of high-spin states in ^{107}Ag have been measured through the Doppler shift attenuation method. The experimental results and theoretical calculations support that band 1 and band 3 in ^{107}Ag exhibit characteristics of magnetic rotation. Furthermore, a systematic investigation shows the evolution of the magnetic rotational mechanism in the $A \approx 110$ mass region. It can be seen that magnetic rotation is active in the $A \approx 110$ mass region due to the occupation of the high-Ω $g_{9/2}$ orbital for the proton hole and the low-Ω $g_{7/2}$, $d_{5/2}$, and $h_{11/2}$ orbitals for neutrons. Moreover, it is evident that the contribution from magnetic rotation increases and the contribution from collective rotation decreases with the growing number of proton towards the proton magic number 50 or with the growing number of $h_{11/2}$ neutrons.

ACKNOWLEDGMENT

The authors thank the crew of the HI-13 tandem accelerator in the China Institute of Atomic Energy for steady operation of the accelerator and for preparing the target. This work is partially supported by the National Natural Science Foundation of China (Grants No. 10775184, No. 10975191, No. 10927507, No. 11075214, and No. 11175259).

[1] Akjain and Deepika Choudhury, Pramana-J. Phys. **75**, 51 (2010).
[2] H. Hübel, Prog. Part. Nucl. Phys. **54**, 1 (2005).
[3] A. Y. Deo *et al.*, Phys. Rev. C **73**, 034313 (2006).
[4] S. Ray *et al.*, Phys. Rev. C **77**, 024305 (2008).
[5] P. Datta *et al.*, Phys. Rev. C **69**, 044317 (2004).
[6] J. Timár *et al.*, Phys. Rev. C **76**, 024307 (2007).
[7] C. Y. He *et al.*, Phys. Rev. C **81**, 057301 (2010).
[8] P. Datta *et al.*, Phys. Rev. C **78**, 021306(R) (2008).
[9] Dan Jerrestam *et al.*, Nucl. Phys. A **577**, 786 (1994).
[10] F. R. Espinoza-Quinones *et al.*, Phys. Rev. C **55**, 1548 (1997).
[11] Zhang Biao *et al.*, Chin. Phys. C **35**, 1009 (2011).
[12] D. C. Radford, Nucl. Instrum. Methods A **361**, 297 (1995).
[13] J. Gascon *et al.*, Nucl. Phys. A **513**, 344 (1990).
[14] J. F. Ziegler, J. P. Biersack, and U. Littmark, *The Stopping and Range of Ions in Solid*, Vol. 1 (Pergamon, New York, 1985).
[15] H. Morinaga and T. Yamazaki, *In-beam Gamma-ray Spectroscopy* (North-Holland, Amsterdam, 1976).
[16] F. Röset, H. M. Fries, and K. Alder, At. Data Nucl. Data Tables **21**, 91 (1978).
[17] S. Frauendorf, Rev. Mod. Phys. **73**, 463 (2001).
[18] S. Frauendorf, Nucl. Phys. A **557**, 259 (1993).
[19] A. Macchiavelli *et al.*, Phys. Lett. B **450**, 1 (1999).

[20] B. G. Carlsson and I. Ragnarsson, Phys. Rev. C **74**, 044310 (2006).
[21] C. Y. He *et al.*, Phys. Rev. C **83**, 024309 (2011).
[22] P. Olbratowski *et al.*, Acta Phys. Pol. B **33**, 389 (2002).
[23] H. Madokoro, J. Meng, M. Matsuzaki, and S. Yamaji, Phys. Rev. C **62**, 061301 (2000).
[24] J. Meng, J. Peng, S.-Q. Zhang, and P.-W. Zhao, Front. Phys. **8**, 55 (2013).
[25] A. V. Afanasjev, D. B. Fossan, G. J. Lane, and I. Ragnarsson, Phys. Rep. **322**, 1 (1999).
[26] B. G. Carlsson and I. Ragnarsson, Phys. Rev. C **74**, 011302 (2006).
[27] T. Bengtsson and I. Ragnarsson, Nucl. Phys. A **436**, 14 (1985).
[28] J. Timár *et al.*, Phys. Rev. C **73**, 011301(R) (2006).
[29] J. Timár *et al.*, Phys. Lett. B **598**, 178 (2004).
[30] P. Banerjee, S. Ganguly, M. K. Pradhan, H. P. Sharma, S. Muralithar, R. P. Singh, and R. K. Bhowmik, Phys. Rev. C **83**, 024316 (2011).
[31] P. Vaska *et al.*, Phys. Rev. C **57**, 1634 (1998).
[32] R. S. Chakrawarthy and R. G. Pillay, Phys. Rev. C **55**, 155 (1997).
[33] S. Naguleswaran *et al.*, Phys. Rev. C **72**, 044304 (2005).
[34] P. Datta *et al.*, Phys. Rev. C **67**, 014325 (2003).